Aust. J. Phys., 1976, **29**, 211–26

Observations of Interstellar CH at 9 cm Wavelength

F. F. Gardner, B. J. Robinson and M. W. Sinclair

Division of Radiophysics, CSIRO, P.O. Box 76, Epping, N.S.W. 2121.

Abstract

The 9 cm ground-state lines of CH have been observed in southern galactic sources, mainly HII regions. The F = 0–1 transition at 3264 MHz has been detected in emission in 16 sources; the F = 1–1 transition at 3335 MHz has been seen in absorption in 5 sources and in emission in 2 others. Where the F = 1–1 transition is in absorption the transition temperature is positive and below about 100 K. The F = 0–1 transition is generally inverted, with a transition temperature between -10 and 0 K. The column densities of CH are in the vicinity of $10^{14}\,\mathrm{cm}^{-2}$, slightly below those for OH but many times those for H_2CO. There is no correlation between apparent optical depths of CH and those for OH or H_2CO absorption. There is also no enhancement of CH in the dense molecular clouds near the centre of the Galaxy.

1. Introduction

The first detection of the 9 cm ground-state lines of CH was reported by Rydbeck *et al.* (1973) from observations with the Onsala 25 m telescope. Because of hyperfine splitting of the ground-state $^2\Pi_{\frac{1}{2}}$, $J = \frac{1}{2}$ Λ-doublet there are three frequencies ν_{01}, ν_{11} and ν_{10} corresponding to the transitions F = 0–1, 1–1 and 1–0, and for uniform excitation and low optical depths their intensities should be in the ratio 1 : 2 : 1. The upper satellite line ν_{10} was detected independently by Turner and Zuckerman (1974), in emission in the direction of Cas A. CH in absorption was first detected with the Parkes 64 m telescope, at the ν_{11} frequency in the direction of the HII region RCW 38 (Robinson *et al.* 1974; hereinafter referred to as Paper I).

At Onsala the three lines have been found in emission with about the expected intensity ratio in the direction of dark clouds and, from a comparison with OH profiles, Rydbeck *et al.* (1974) gave the rest frequencies (in MHz) as

$$\nu_{01} = 3263\cdot794\pm0\cdot003\,, \qquad \nu_{11} = 3335\cdot481\pm0\cdot002\,, \qquad \nu_{10} = 3349\cdot193\pm0\cdot003\,.$$

These values are used in this paper. Subsequently Zuckerman and Turner (1975) have compared CH, H_2O and OH spectra for four sources and determined rest frequencies of 3263·793, 3335·478 and 3349·192 MHz. The small differences between the two sets of rest frequencies are insignificant for our observations.

In the direction of strong galactic continuum sources there are large departures from the LTE ratio of intensities, although at Onsala all three lines were generally seen in emission. It is common for the 3264 MHz line to be enhanced to the point where it is the strongest of the three. The 3349 MHz transition is always in emission, while the 3335 MHz line was found in absorption in one case in our first observations. The observations to be described in this paper were made in January 1974. As the system noise was some five times higher than the value of about 40 K achieved at Onsala with a travelling wave maser, we concentrated on observations towards HII regions where the increased gain of the Parkes 64 m telescope might offset in part the higher noise. The present results have been summarized by Gardner and Robinson (1974).

2. Observations

The observations were made with the Parkes 64 m telescope (beam $\sim 6' \cdot 4$ arc). The first stage of the receiver was an uncooled parametric amplifier with an instantaneous bandwidth of about 30 MHz, which could be tuned over the range 3·1–3·5 GHz. The system noise temperature on cold sky was about 200 K. Dicke switching against a sky-horn reference was employed, with noise being added to the reference for balance in the continuum. The multichannel backend, which has 64 contiguous filters with bandwidths of 1, 10, 33 or 100 kHz, was used, mostly with the 10 kHz filters. The filter spacing of 9·5 kHz corresponds to 0·85 $\mathrm{km\,s^{-1}}$ in radial velocity, and the velocity coverage of the 10 kHz filter bank is 57 $\mathrm{km\,s^{-1}}$. The recording and normalizing of the spectra were under the control of a PDP 9 computer with a program developed by J. C. Ribes. The recordings were mostly made using an off-source observation as reference, but in some cases a second on-source observation, taken with a small change in local oscillator frequency, was used. The latter improved the sensitivity but reduced the effective velocity coverage.

In terms of the noise calibration and an assumed point-source flux density for Hydra A of 19·2 Jy* at 3·3 GHz, the aperture efficiency was 55% and the beam efficiency 70%.

Most observations were made at the F = 0–1 frequency. If this line was detected, the F = 1–1 transition ν_{11} was usually observed. Only in a few cases was an attempt made to detect the remaining frequency ν_{10}, since on the basis of the Onsala data and our previous results it was expected to be weaker than our sensitivity limit. The sources observed were mostly HII regions, and integration times between 20 and 60 min were usual.

3. Results

(*a*) *General*

The results are summarized in Table 1. Most of the column headings are self-explanatory. Line and continuum intensities are given as antenna temperatures (multiplication by 1·22 converts to a scale of full-beam brightness temperature). The CH line parameters were estimated from the spectra. Errors quoted are approximately half the peak-to-peak noise (2σ). The ratio T_L/T_c in column 12 is that of the line peak temperature T_L to the continuum temperature T_c. The comparison velocities in OH, H_2CO and recombination lines were compiled from Parkes data for a previous publication (Whiteoak and Gardner 1974) where the sources of information are referenced and additional information on optical depths is provided.

(*b*) T_L/T_c *for CH*

At ν_{01} (3264 MHz) T_L/T_c lies between 0·01 and 0·08. Because only upper limits are available in several cases the average is uncertain but the median value is 0·021. At ν_{11} (3335 MHz) the median T_L/T_c for the absorption cases is $-0 \cdot 010$. Because of

* 1 Jy (jansky) = $10^{-26}\,\mathrm{W\,m^{-2}\,Hz^{-1}}$.

our sensitivity limit it is not possible in this case to make a meaningful estimate of the true T_L/T_c average for all sources, although on the basis of the Onsala data we would expect that it would be positive.

A search was made for possible association between T_L/T_c for CH at 3264 MHz and similar ratios for OH and H_2CO absorption (from Table 1 of Whiteoak and Gardner 1974). There was no significant correlation in either case. The mean value of the ratio of T_L/T_c(CH) to T_L/T_c(OH) was $-0{\cdot}20$ with $\sigma = 0{\cdot}14$. The highest ratio was $0{\cdot}46$ for G265·5+1·5 (RCW 36). The mean value of the ratio of T_L/T_c(CH) to T_L/T_c(H_2CO) was $-0{\cdot}37$ with $\sigma = 0{\cdot}23$. Numerically the highest ratio was $0{\cdot}84$ for the peak of NGC 6334 at a velocity of $-4\ \mathrm{km\,s^{-1}}$. In all these comparisons of T_L/T_c, and for the velocities in the next subsection, the galactic centre sources were excluded.

(c) *Radial Velocities for CH*

An examination of Table 1 reveals that the CH velocities are usually close to those of OH, H_2CO and the recombination-line velocity of the HII region. In only two cases is a second velocity component observed well separated from that of the HII region. If these are excluded (since the second component would be associated with another region of the Galaxy) the mean OH–CH velocity difference (1667 MHz OH absorption and 3264 MHz CH emission) is $-0{\cdot}01\ \mathrm{km\,s^{-1}}$ with $\sigma = 1{\cdot}1\ \mathrm{km\,s^{-1}}$. The mean H_2CO–CH difference is $-2{\cdot}1\ \mathrm{km\,s^{-1}}$ with $\sigma = 3{\cdot}7\ \mathrm{km\,s^{-1}}$. The mean recombination-line–CH difference is $-0{\cdot}9\ \mathrm{km\,s^{-1}}$ with $\sigma = 2{\cdot}3\ \mathrm{km\,s^{-1}}$. The velocity association is closer between CH and OH than between CH and either H_2CO or the recombination lines.

(d) *Comparison of $F = 0$–1 and $F = 1$–1 Lines*

Of the total of five sources showing absorption at ν_{11}, four were observed at ν_{01}. The velocity differences $(V_{11}-V_{01})$ were $-3{\cdot}1$, 0, $-0{\cdot}9$ and $-0{\cdot}3\ \mathrm{km\,s^{-1}}$ and the mean difference $-1{\cdot}1\ \mathrm{km\,s^{-1}}$. The largest difference, $-3{\cdot}1\ \mathrm{km\,s^{-1}}$ for RCW 38, was discussed by Robinson *et al.* (1974). For the same five sources the average T_L/T_c ratio was $-0{\cdot}010$ at 3335 MHz and $0{\cdot}026$ at 3264 MHz. The average of the individual ratios $T_L(\nu_{01})/T_L(\nu_{11})$ was $-2{\cdot}5$, to be compared with the LTE value of $0{\cdot}5$.

We have previously (Gardner and Robinson 1974) commented on a possible connection between the occurrence of absorption at ν_{11} and the peak emission measure *E.M.* (and brightness temperature T_c) of the HII region. Four of the five sources in Table 2 (reproduced from Gardner and Robinson) with absorption at ν_{11} have peak brightness temperature T_c exceeding 1000 K. Of the eight for which the ν_{11} signal was either undetectable or showed weak emission, seven had T_c below 230 K. The exception was Orion, with $T_c = 950$ K. However, it is known (Kutner and Thaddeus 1971) that in this case the molecular cloud is behind the continuum source and probably associated with the IR nebula, the radio continuum brightness of which would certainly be below 230 K.

(e) *Results for Individual Sources*

G206·5−16·4 (*NGC 2024, W12*). The velocity agreement with OH and H_2CO is good. The value of T_L/T_c(3264) at $0{\cdot}022$ is near the average, although for both OH and H_2CO the optical depths are the largest of the sources investigated for CH.

Table 1. Summary of CH results

Entries in columns 7, 9, 10, and 11 are in units of km s^{-1}

(1) Source designation: G number	(2) Source designation: Other	(3) Position (1950): R.A. h m s	(4) Position (1950): Dec. ° ′	(5) Cont. T_c (K)	(6) Freq. (MHz)	(7) Vel. range searched	(8) CH data: T_L (K)	(9) CH data: Half-width	(10) CH data: Rad. vel.	(11) CH data: Total extent	(12) CH data: $\frac{T_L}{T_c}$	(13) Comparison velocities (km s^{-1}): OH	(14) Comparison velocities (km s^{-1}): H_2CO	(15) Comparison velocities (km s^{-1}): HII
206·5−16·4	NGC 2024, W12	05 39 12	−01 56·2	32	3264	−16,38	0·7±0·2	2·2	9·7		0·022	9·3	9·3	6·5
265·5+1·5	RCW 36	08 57 39	−43 33·7	11·1	3264	−22,32	0·85±0·15	~4	6·7	0,10	0·077	6	3·7	2·8
						3,9^A	{1·0±0·2	0·6	6·67		0·090		6·7	
							{0·6±0·2	—	4·84		0·054			
					3335	−21,31	0·3±0·15	6	6·4		0·027			
267·8−0·9	RCW 38	08 57 42	−47 07·6	6·5	3264	−22,32	<0·15				<0·023		4·9	
					3335	−21,31	⩽0·15				⩽0·023			
267·9−1·1	RCW 38													
Peak		08 57 25	−47 19·6	89	3264	−25,29	1·85±0·2	6·1	3·1	−4,6·5	0·021	2	2·8	1·8
3′S.		08 57 25	−47 22·6	51			0·96±0·15				0·019		4·4	
3′N.		08 57 25	−47 16·6	54			1·16±0·15				0·021			
18^s E.		08 57 43	−47 19·6	57			0·90±0·15				0·016			
17^s W.		08 57 08	−47 19·6	50			0·88±0·15				0·018			
Peak		08 57 25	−47 19·6	89	3335	−24,28	−0·58±0·15	3·2	0·0	−12,4	−0·0065			
3′·3S.		08 57 25	−47 22·9	51			−0·32±0·15				−0·0063			
3′·3N.		08 57 25	−47 16·3	48			−0·27±0·15				−0·0055			
17^s E.		08 57 42	−47 19·6	49			−0·33±0·15				−0·0066			
268·0−1·0	RCW 38	08 58 07	−47 20·4	9·7	3264	−22,32	<0·15				<0·016		4·4	
				8·2	3335	−21,31	<0·15				<0·016			
284·2−0·8		10 19 44	−57 50·3	1·3	3264	−52,2	<0·15				<0·12	−25^B		
291·3−0·7	RCW 57, NGC 3576	11 09 47	−61 02·9	53	3264	−52,2	0·72±0·15	4·0	−26·1	−37,−20	0·014	−26	−25·8	−23·4
					3335	−50,0	−0·30±0·15	6·0	−26·1		−0·006		−21·6	
291·6−0·5	RCW 57, NGC 3603	11 12 53	−60 59·4	69	3264	−12,40	0·3±0·2	2·0	1·8		0·004?	12	−27·2	9·8
					3335	−11,40	<0·2				<0·003			
291·6−0·4	NGC 3603	11 12 53	−60 55·4	41	3264	−12,40	0·3±0·2	2·4	2·0		0·007?	15^B	−27·8	
316·8+0·0	HII	14 41 30	−59 37·2	17·6	3264	−64,12	0·33±0·1	7·5	−39·5	−47,−35	0·019	−39	−45·9	−36·1
					3335	−63,12	0·07±0·05	~7	−44·5		0·004		−37·1	
326·7+0·6	HII	15 40 59	−53 57·7	17·3	3264	−80,−2	{0·27±0·07	3·5	−43·5	−50,−40	0·016	−46	−54·2	−44·5
							{0·31±0·1	2·2	−21·3		0·018	−21	−21·7	
					3335	−70,−20	<0·14				<0·008			

327·3−0·5	HII	15 49 12	−54 26·6	26·5	3264	−74, −22	0·81±0·15	5·7	−49·4		0·031	−50	−48·7	−48·8
					3335	−74, −22	−0·36±0·15	3·6	−50·3		−0·014			
					3349	−74, −22	−0·2±0·2	—	−50·0		−0·008?			
	(−21^s, −3′)	15 48 51	−54 29·6	12·2	3264	−74, −22	0·35±0·15	5·9	−48·7		0·029			
330·9−0·4		16 06 32	−51 58·4	5·9	3264	−87,36	0·13±0·13	12	−66		0·022?	−63·5[B]	−62·7	−56·1
							0·21±0·15	3	−57·8		0·036?		−49·6	
331·5−0·1	HII	16 08 21	−51 19·6	18·2	3264		0·57±0·2	5·5	−89·3	−98, −91	0·031	−92[B]	−89·3	−88·7
333·6−0·2	HII	16 18 26	−49 59·1	42	3335	−87,36	−0·44±0·2	⩾4·3	−54·8		−0·010	−52[B]	−45·8	−48·3
												−42	−39·9	
351·1+0·7	NGC 6334B	17 16 36	−35 55·2	12·7	3335	−34,16	<0·14				<0·011	−7·9[B]	−6·7	−3·6
351·4+0·7	NGC 6334 peak	17 17 11	−35 46·9	41	3264	−33,18	1·53±0·2	3·9	−4·3		0·037	−4·5	−3·5	−3·2
							0·35±0·2	—	7·0		0·009	5·5	6·5	
					3335	−35,15	−0·61±0·2	3·4	−4·6		−0·015			
351·4+0·6	NGC 6334A	17 17 34	−35 43·7	24·1	3264	−33,18	0·83±0·2	4·5	−4·2		0·034	−12[B]	−5·0	(−3·2)
				19·7	3335	−33,18	⩽0·14±0·14				⩽0·007			
359·9−0·1	Sgr A	17 42 31	−28 59·1	126	3264	−100,100[C]	0·56±0·1	~6	−51·9		0·0044		−52·0	
							0·31±0·1	~6	−29·0		0·0025		−30·0	
							0·94±0·1	14	−1·4		0·0075		−4·8	
							0·21±0·1	34	35·0	20,70	0·0017		43·0	
							0·28±0·1	11	55·2		0·0022			
					3335	−100,100[C]	Lines present[D]			−55,60				
					3349	−100,100[C]	⩽0·15							
359·9−0·1	Sgr A (6′S.)	17 42 31	−29 05·1	26	3264	−100,100[C]	0·23±0·07		−53·2		0·0088			
							0·27±0·07	13	2·4		0·0104			
							0·15±0·07	32	33·1		0·0058			
0·0+0·0	Sgr A (6′N.)	17 42 31	−28 53·1	41	3264	−100,100[C]	0·23±0·1	~6	−51·9		0·0049			
							0·91±0·1	7	0·6		0·0194			
							0·17±0·1	50	43·8		0·0036			
0·1−0·0		17 42 36	−28 51·5	39	3264	−100,100[C]	0·28±0·1	9	−29·0		0·0072		−29·1	−39·9
							0·67±0·1	9	1·0		0·0172		0·2	11·1
							0·22±0·1	21	36·2		0·0056			
0·7−0·0	Sgr B2	17 44 11	−28 22·6	25	3264	−100,100[C]	0·09±0·09	15	1·1		0·0036?		3·4	61·7
							0·40±0·09	20	65	40,75	0·0160	67·3[B]	62·7	

[A] Obtained with 1 kHz filters.
[B] Line appeared as maser emission.
[C] Obtained with 33 kHz filters.
[D] See results for individual sources in Section 3*e*.

From Paper I, $T_L/T_c(3335)$ was $+0\cdot007$; it was also found that $T_L(3335)$ at a position 5′ arc to the south, where the continuum had fallen to 0·15 of its peak value, had only decreased to 0·7 of the peak value, which indicates that the CH cloud is considerably greater in extent than the continuum.

G265·1+1·5 (*RCW36*). The emission at 3264 MHz extended from about 0 to 10 km s^{-1} and only the central portion, smoothed to 2 kHz resolution, is shown in Fig. 1. The line shows fine structure under 1 km s^{-1}, the narrowest observed. At 3335 MHz the line was in emission, and the observations of Paper I showed that this emission was of greater extent than the continuum.

Table 2. CH at 3335 MHz (F = 1 → 1)

Sources with no absorption	*E.M.* (peak) (pc cm^{-6})	T_c (peak) (K)	Sources with absorption	*E.M.* (peak) (pc cm^{-6})	T_c (peak) (K)
G206·5−16·4 (NGC 2024)	$7\cdot9\times10^5$	198	G267·9−1·1 (RCW 38)	$6\cdot5\times10^6$	1620
G209·9−19·4 (Orion A)	$3\cdot8\times10^6$	(950)	G291·3−0·7	$8\cdot3\times10^6$	2075
G265·1+1·5 (RCW 36)	$4\cdot5\times10^5$	112	G327·3−0·5	$4\cdot4\times10^6$	1100
G291·6−0·5	$7\cdot5\times10^5$	187	G333·6−0·2	$7\cdot1\times10^6$	1775
G316·8+0·0	$9\cdot0\times10^5$	224	G351·4+0·7 (NGC 6334)	$3\cdot1\times10^5$	(78)
G326·7+0·6	$3\cdot4\times10^5$	85			
G331·5−0·1	$5\cdot7\times10^5$	142			
G0·7−0·0 (Sgr B2)	$5\cdot2\times10^5$	130			

G267·9−1·1 (*RCW38*). Fig. 1 of Paper I shows emission at 3264 MHz, absorption at 3335 MHz and probably weak emission at 3349 MHz. Because of the revised rest frequencies for the lines, the velocities used in Paper I should be increased by about 0·7 km s^{-1}. New observations at 3264 and 3335 MHz are given in the present Fig. 2, where it can be seen that of two possible components in the 3264 MHz profile only one appears to show as absorption. In detail the CH(3264) profile agrees better with the OH(1667) than with the H_2CO. The weak and broad 3335 MHz emission centred near −10 km s^{-1} is in agreement with the spectrum in Paper 1.

Additional observations were made at positions to the north, south, east and west of the continuum peak at both 3264 and 3335 MHz. Within the accuracy limits, the decrease in T_L was proportional to the decrease in T_c, a result consistent with the radio continuum being absorbed at 3335 MHz and amplified at 3264 MHz by an overlying cloud of CH of angular extent equal to or greater than that of the continuum, although any beam broadening at 3335 MHz is small. If there were indeed no broadening the absorption could be produced by a very small cloud.

G291·3−0·7 (*NGC 3576*). In Fig. 3 there is emission at 3264 MHz and absorption at 3335 MHz. The 3264 MHz profile indicates a narrow component near the centre of a wider one. At 3335 MHz there is a suggestion of a second weaker component at −40 km s^{-1}; this is probably spurious as no HI, OH or H_2CO has been observed at this velocity.

G291·6−0·5 and G291·6−0·4 (*NGC 3603*). CH was not definitely detected at either position. The second position is near an OH emission centre.

G316·8+0·0. There is good agreement in velocity between CH(3264), OH and the stronger H_2CO component.

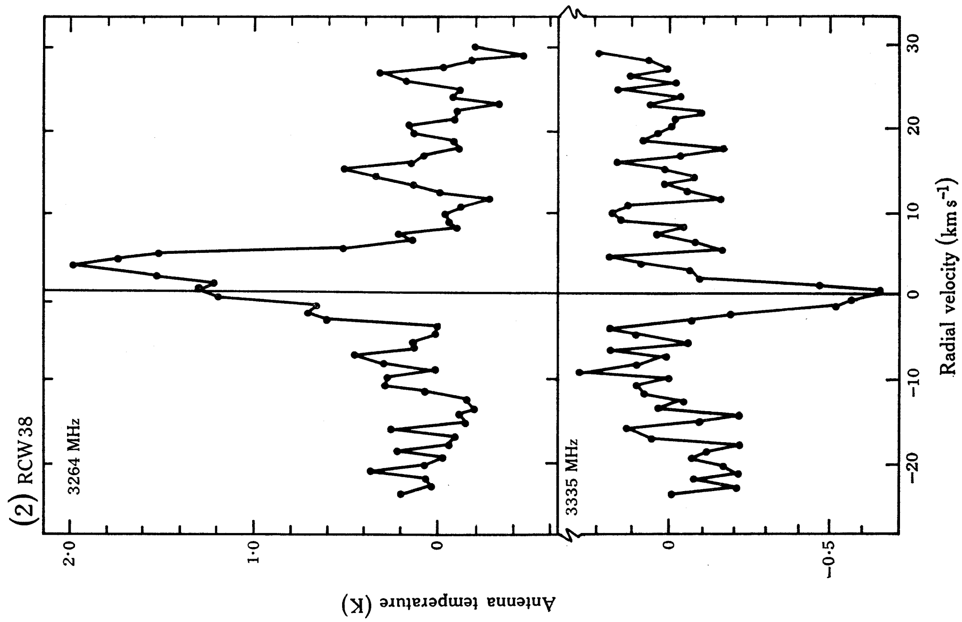

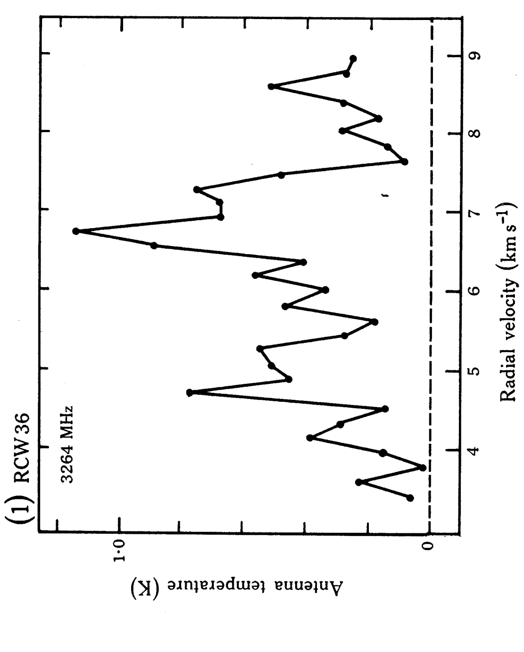

Fig. 1. CH line profile for the F = 0–1 transition in the direction of RCW 36. The plotted points are 2 kHz ($\approx$0·2 km s^{-1}) apart.

Fig. 2 (*right*). CH line profiles for the F = 0–1 and 1–1 transitions in the direction of RCW 38. The channel spacing is 9·5 kHz ($\approx$0·85 km s^{-1}).

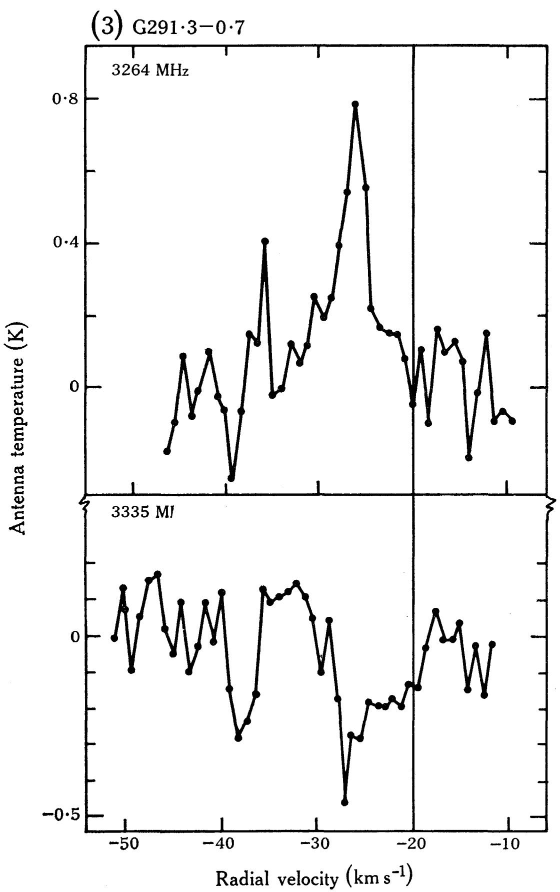

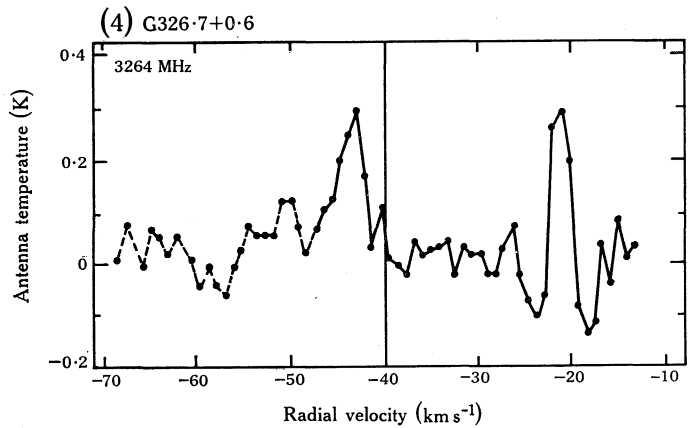

Fig. 3 (*left*). CH line profiles for the F = 0–1 and 1–1 transitions in the direction of G291·3−0·7. The channel spacing is 9·5 kHz ($\approx 0{\cdot}85\ \mathrm{km\,s^{-1}}$).

Fig. 4 (*above*). CH line profile for the F = 0–1 transition in the direction of G326·7+0·6. The profile is the average of two taken with different local oscillator settings; the non-overlapping portion is shown dashed. The channel spacing is 9·5 kHz ($\approx 0{\cdot}85\ \mathrm{km\,s^{-1}}$).

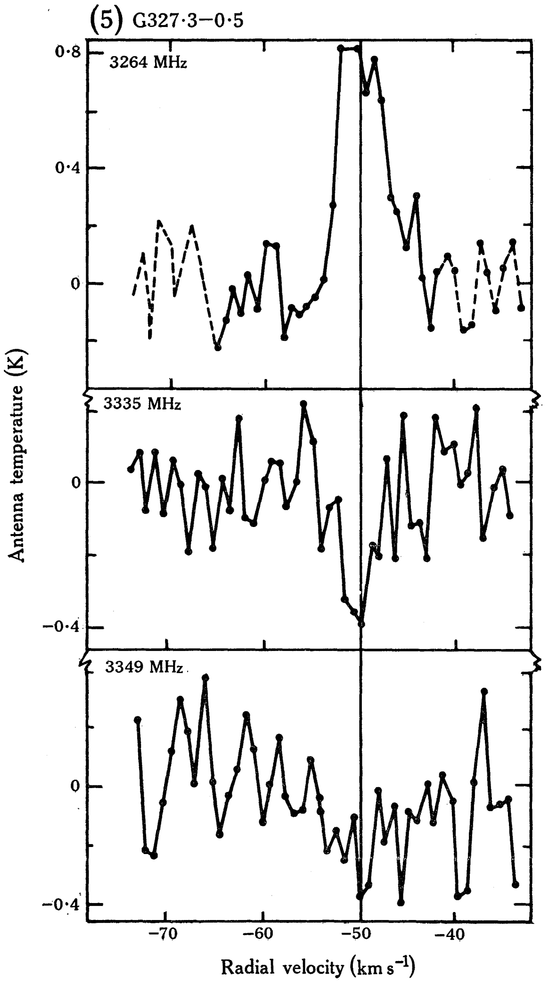

Fig. 5. CH line profiles for the F = 0–1, 1–1 and 1–0 transitions in the direction of G327·3−0·5. The F = 0–1 profile is the average of two taken with different local oscillator settings; the non-overlapping portion is shown dashed. The channel spacing is 9·5 kHz ($\approx 0\cdot 85$ km s^{-1}).

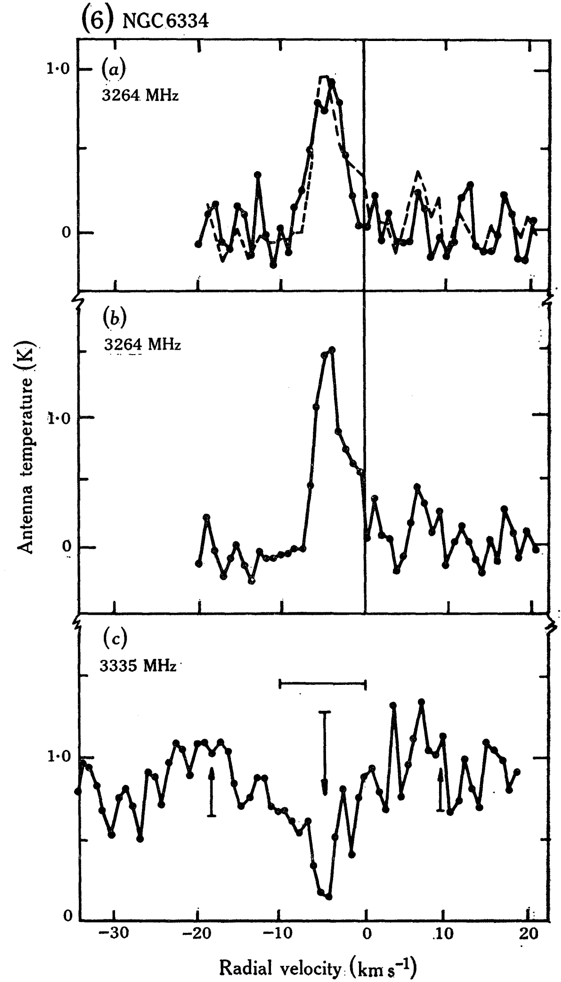

Fig. 6 (*right*). CH line profiles for the F = 0–1 transition in the direction of (*a*) the OH emission centre NGC6334A and (*b*) the continuum peak of NGC6334. The profile (*b*) reduced in amplitude is shown superposed as the dashed curve on (*a*). The profile (*c*) is for the F = 1–1 transition towards the continuum peak. The arrows indicate the locations and relative amplitudes for absorption at a velocity of -4 km s^{-1} (see text).

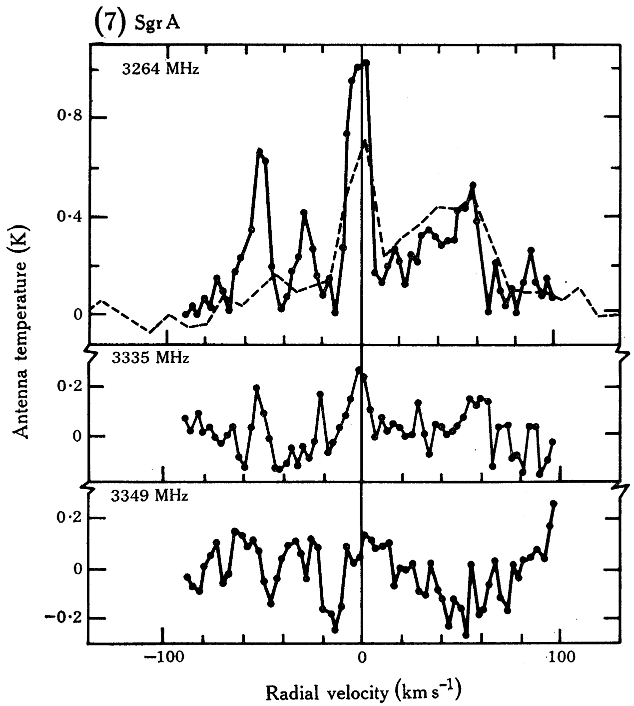

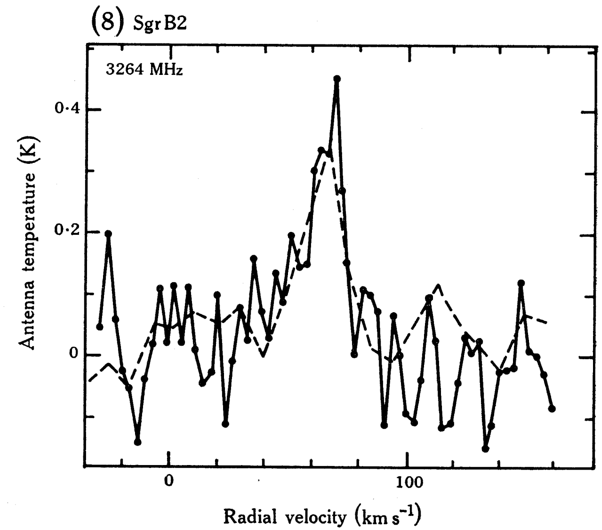

Fig. 7. CH line profiles for the F = 0–1, 1–1 and 1–0 transitions in the direction of Sgr A. The filter bandwidth is 33 kHz (≈ 3 km s^{-1}) for the continuous curves and 100 kHz for the dashed curve.

Fig. 8. CH line profile for the F = 0–1 transition in the direction of Sgr B2. The filter bandwidth is 33 kHz for the continuous curve and 100 kHz for the dashed curve.

G326·7+0·6. At 3264 MHz there is (Fig. 4) emission at $-43\ \mathrm{km\,s^{-1}}$, near the recombination line velocity of $-44\ \mathrm{km\,s^{-1}}$, and also at $-21\ \mathrm{km\,s^{-1}}$. The latter must occur in a spiral feature closer to the Sun than the one containing the HII region. The second velocity component is also present in absorption at OH and CH. The large difference of $10\cdot7\ \mathrm{km\,s^{-1}}$ between the CH and H_2CO velocities of $-43\cdot5$ and $-54\cdot2\ \mathrm{km\,s^{-1}}$ is probably a consequence of the very wide H_2CO absorption (which extends from -60 to $-17\ \mathrm{km\,s^{-1}}$) and the lack of correspondence between T_L/T_c in CH and H_2CO (see subsection (*b*) above).

G327·3−0·5. As shown in Fig. 5, there is strong emission at 3264 MHz and absorption at about the same velocity at 3335 MHz, while there is a suggestion of weak absorption at about the same velocity at 3349 MHz. The last should be reobserved, since it would be the first case of absorption of the F = 1–0 transition. An additional observation was made of the 3264 line at a position $4'\cdot5$ arc to the south-west of the continuum peak, along the direction of extension of the source. The T_L/T_c ratio at the offset position is the same as at the peak, similar to the result obtained for RCW 38.

G330·9−0·4. The position is near a very strong OH emitter. No definite detection of CH was made.

G351·4+0·7 (NGC 6334 peak), G351·4+0·6 (NGC 6334A), G351·1+0·7 (NGC 6334B). At the continuum peak there is strong emission at 3264 MHz and absorption at 3335 MHz. For the 3335 MHz profile in Fig. 6*c* the reference spectrum was the average of two spectra displaced ± 152 kHz ($\pm 14\ \mathrm{km\,s^{-1}}$) from the signal spectrum. For absorption we should expect signals of $\frac{1}{2}$, -1 and $\frac{1}{2}$ spaced by $14\ \mathrm{km\,s^{-1}}$, similar to what is observed. Observations were also made at the OH emission centres, NGC 6334A at 3264 and 3335 MHz, and NGC 6334B at 3335 MHz only. Superimposed as a dashed curve on the 3264 MHz profile of NGC 6334A in Fig. 6*a* is the profile (*b*) at the peak, reduced by the continuum ratio for the two positions. Although there does appear to be some difference in shape between the profiles shown by full and dashed lines, the peak values and the areas are similar, indicating again that the CH amplification is about the same at positions 6′ arc apart. No 3335 MHz signal was detected at NGC 6334A, suggesting that the absorbing cloud is smaller than the continuum source. It can be seen from Table 2 that NGC 6334 was the only low-brightness source with 3335 MHz absorption.

G359·9−0·1 (Sgr A), G0·1−0·0 and G0·7−0·0 (Sgr B2). These are sources near the galactic centre. For Sgr A (Fig. 7) there is strong emission at 3264 MHz for velocities of -50, -30 and $0\ \mathrm{km\,s^{-1}}$, plus a weaker broader line at $\sim 40\ \mathrm{km\,s^{-1}}$ which could comprise a narrow and a wide component as given in Table 1. At 3335 MHz, lines at -50, 0 and possibly $50\ \mathrm{km\,s^{-1}}$ can be distinguished while, at 3349 MHz, no feature clearly exceeds the noise.

Additional 3264 MHz observations were made at positions $\pm 6'$ arc in declination from the Sgr A continuum peak, and also towards the source G0·1−0·0. The $0\ \mathrm{km\,s^{-1}}$ feature shows a clear displacement of 2′ to 3′ arc to the north of Sgr A, but more detailed mapping is required for any estimate of the cloud size. There is no obvious displacement of the -50 and $40\ \mathrm{km\,s^{-1}}$ features.

In Sgr B2 the only strong line was in emission at 3264 MHz. The profile peak in Fig. 8 is at $64\ \mathrm{km\,s^{-1}}$, close to the OH, H_2CO and HII velocities.

4. Discussion

(*a*) *Size of CH Clouds*

The data at present available on cloud sizes are very limited and in our observations are restricted to clouds which may be associated with HII regions. The size of the clouds emitting the F = 1–1 frequency of 3335 MHz must usually be larger than the continuum sources, and larger than our beam of 6′ arc. This is shown from our observations of RCW 36 and NGC 2024, and by the fact that our antenna temperatures are not much greater than those at Onsala (the ratio is certainly well below 6, the ratio of the gains of the two telescopes). The clouds producing the absorption at 3335 MHz could be the same as those appearing in emission, as the observed sizes are largely determined by the sizes of the continuum sources behind the CH clouds. However, it is possible that the absorbing clouds are smaller. The profiles of the absorption at 3335 MHz are usually narrower than for the emission at 3264 MHz, which suggests that only some clouds absorb, and in NGC 6334 the observations indicate that the absorbing cloud is smaller than the continuum source. As yet there is no case of 3335 MHz absorption at a velocity well separated from that of the HII region.

Amplification at the F = 0–1 frequency of 3264 MHz appears to be a general feature of CH sources. The intensity in the neighbourhood of the source decreases in proportion to the fall in the continuum. Onsala results show that amplification at 3264 MHz also occurs in regions well separated from the continuum source. At the F = 1–0 frequency of 3349 MHz there is essentially no information on cloud sizes.

(*b*) *Distribution of CH Clouds*

Our results are consistent with the Onsala conclusion that CH is widely distributed in the Galaxy, although probably restricted to spiral arms. The CH observations of Sgr A provide some information on this point. Except for the reversal in sign, the 3264 and 3335 MHz CH profiles resemble the 21 cm absorption profiles of neutral hydrogen rather than the spectra of other molecular lines. The profiles of OH, H_2CO etc. are dominated by a strong feature at 40 km s^{-1} which is believed to be a dense molecular cloud close to the centre (see e.g. Robinson 1974). For such molecules the features at -50, -30 and 0 km s^{-1}, which are believed to arise in spiral arms between the Sun and the galactic centre, are not conspicuous. Thus it appears that the density of CH near the galactic centre is not enhanced relative to that in the intervening arms. This suggests that in the dense 40 km s^{-1} cloud the CH has been used up in the formation of more complex molecules, such as formaldehyde and methyl alcohol. The paucity of CH in dense molecular clouds is supported by the lack of correlation between $T_{\mathrm{L}}/T_{\mathrm{c}}$ (CH) with similar ratios for OH and H_2CO. Finally it would be expected that the CH–HI association would only be with the colder denser clouds of neutral hydrogen.

(*c*) *Excitation and Column Densities of CH*

For low optical depths the line integral of the brightness temperature $T_{\mathrm{b}}(V)$ across the profile may be written, for each line, as

$$\int T_{\mathrm{b}}(V)\,\mathrm{d}V = \frac{hc^3 A_{ul}}{8\pi k\nu^2}\int n_{\mathrm{u}}\,\mathrm{d}l\left(1-\frac{T_{\mathrm{c}}}{T_{\mathrm{tr}}}\right), \qquad (1)$$

where V is the velocity, A_{ul} the Einstein coefficient for spontaneous emission, n_u the population of the upper level, T_c the brightness temperature of the continuum behind the CH cloud and T_{tr} the effective temperature of the transition. The A coefficients have been calculated by Burdyuzha and Varshalovich (1973) and Turner and Zuckerman (1974). Their results are essentially in agreement and correspond to $A = 1{\cdot}94 \times 10^{-10}\,\mathrm{s}^{-1}$ for $\nu_{11} = 3335{\cdot}5$ MHz.

If $\int N\,\mathrm{d}l$ is the total column density (per cm^2) of the four levels of the $^2\Pi_{\frac{1}{2}}$, $J = \frac{1}{2}$ state then (for V in $\mathrm{km\,s^{-1}}$) equation (1) becomes

$$\int T_{\mathrm{b},ij}(V)\,\mathrm{d}V = K_{ij}\int N\,\mathrm{d}l\left(1-\frac{T_\mathrm{c}}{T_{ij}}\right), \tag{2}$$

where T_{ij} is the transition temperature and the K_{ij} for ν_{11}, ν_{01} and ν_{10} are respectively

$$K_{11} = 3{\cdot}36\times10^{-15}, \qquad K_{01} = 1{\cdot}75\times10^{-15}, \qquad K_{10} = 1{\cdot}66\times10^{-15}.$$

The relationship between the observed antenna temperature and T_b depends on the geometry of the molecular cloud and the continuum source. For the simplest model, where the source and cloud are uniform discs subtending angles Ω_s and Ω_cl at the Earth and the antenna beam solid angle is Ω_B, we can distinguish four cases:

(i) When Ω_B is the smallest, the full-beam brightness temperature will be equal to T_b.

(ii) When Ω_cl is the smallest, the apparent brightness temperature will be reduced to $T_\mathrm{b}\,\Omega_\mathrm{cl}/\Omega_\mathrm{B}$.

(iii) With $\Omega_\mathrm{s} < \Omega_\mathrm{cl} < \Omega_\mathrm{B}$, equation (2) is modified to

$$\int T_{\mathrm{b},ij}(V)\,\mathrm{d}V = K_{ij}\int N\,\mathrm{d}l\,\frac{\Omega_\mathrm{cl}}{\Omega_\mathrm{B}}\left(1-\frac{T_\mathrm{c}}{T_{ij}}\frac{\Omega_\mathrm{s}}{\Omega_\mathrm{cl}}\right). \tag{3}$$

(iv) With $\Omega_\mathrm{s} < \Omega_\mathrm{B} < \Omega_\mathrm{cl}$,

$$\int T_{\mathrm{b},ij}(V)\,\mathrm{d}V = K_{ij}\int N\,\mathrm{d}l\left(1-\frac{T_\mathrm{c}}{T_{ij}}\frac{\Omega_\mathrm{s}}{\Omega_\mathrm{B}}\right), \tag{4}$$

in which $T_\mathrm{c}\,\Omega_\mathrm{s}/\Omega_\mathrm{B}$ is the apparent brightness temperature of the continuum source.

(*d*) *CH in Dark Clouds*

Hjalmarson *et al.* (1975) have detected CH emission lines towards more than 100 positions in optically dark nebulae. Such clouds would be case (i) or case (ii) above. They have observed all three CH transitions in emission in the direction of the extragalactic source 3C 123, which lies behind the dust cloud Lynds 1500, and have been able to deduce values of T_{ij}. They find that the CH transitions are all inverted with $T_{11} \approx -9\,K$, $T_{10} \approx -6$ K and $T_{01} \approx -5$ K. Thus the fractional inversion (proportional to $-T_{ij}^{-1}$) is greater for the satellite lines than the main line. Inversion of the transition is also deduced from the observations of the CH cloud which lies in front of 3C 353. For Lynds 1500, Hjalmarson *et al.* find $\int N_\mathrm{CH}\,\mathrm{d}l \approx 10^{14}$ molecules cm^{-2}.

(e) CH associated with HII Regions

In the CH clouds associated with HII regions we have observed absorption at ν_{11} in sources where T_c exceeds 1000 K. The line appears weakly in emission for sources with T_c less than 250 K (see Table 2). The ν_{01} transition is always in emission, and is much stronger than the ν_{11} transition. The ν_{10} transition, when seen, is also in emission, although considerably weaker than the ν_{01} line.

Where the ν_{11} transition is in absorption, T_{11} is positive and less than about 1000 K. If Ω_s is smaller than Ω_{cl} and Ω_B, this limit on T_{11} will be reduced by Ω_s/Ω_{cl} in case (iii) above or by Ω_s/Ω_B in case (iv). The latter case will be the most likely situation if the CH clouds observed in absorption with the Parkes 6′ arc beam are of the same type as those observed in emission with the Onsala 16′ arc beam. (None of the sources showing absorption at Parkes has been covered by the Onsala survey.) In case (iv) an absorption line indicates $T_{11} < T_c\,\Omega_s/\Omega_B$, the apparent brightness temperature of the continuum source (see equation 4). For most of the sources in Table 2 we estimate that T_{11} would then be less than 100 K. Thus NGC 6334, with a peak brightness of $\sim$80 K in Table 2, need not be an exception provided that the cloud was large and uniformly excited.

In the continuum sources where we have found absorption at ν_{11} and strong emission at ν_{01}, the ratio $T_{b,01}/T_{b,11}$ is about $-2{\cdot}5$. For $|T_c/T_{ij}| > 1$ we find from equation (2) that T_{01}/T_{11} is $\sim 0{\cdot}5\, T_{b,11}/T_{b,01}$. Thus if T_{11} is approximately +50 K we will have $T_{01} \approx -10$ K, if it is assumed that the clouds producing amplification at ν_{11} are the same as those producing amplification at ν_{01} (possible size differences between these clouds were commented on in Section 4*a* above). The value of $T_{01} \approx -10$ K is similar to the transition temperatures deduced from the Onsala emission data.

In our observations the highest T_L/T_c is measured at 3264 MHz towards RCW 36. For $T_{01} \approx -10$ K the column density is approximately equal to 10^{15} cm^{-2}. This is close to the column density determined for OH by Manchester *et al.* (1970) on the assumption of a transition temperature for OH of 10 K. The H_2CO observations of Whiteoak and Gardner (1974) lead to $\int n_{H_2CO}\,dl \approx 3\times 10^{13}$ cm^{-2} in the direction of RCW 36. Thus the relative abundances of CH, OH and H_2CO are roughly

$$N_{CH}:N_{OH}:N_{H_2CO} \approx 1:1:0{\cdot}03\,.$$

If the CH transition temperature T_{01} were about -5 K the CH column density would be halved.

The possibility of a change in T_{11} from negative to positive values in the vicinity of bright emission sources was postulated previously (Gardner and Robinson 1974) as resulting from an increase in density. However, the lack of correlation between the apparent optical depth of CH and that of OH or H_2CO suggests that, in the denser clouds with high opacity for OH and H_2CO, the CH concentration is low. It is worth noting that, according to the pumping theory of Gwinn *et al.* (1973), collisions between H or H_2 and CH should produce anti-inversion (Turner and Zuckerman 1974). Other pumping mechanisms are discussed by Turner and Zuckerman and by Zuckerman and Turner (1975) without any real conclusions being reached. They do point out, however, that because the next higher states of CH ($^2\Pi_{1/2}, J = 3/2$ and $^2\Pi_{3/2}, J = 3/2$) are only 18 and 67 cm^{-1} above the ground state CH could be pumped at lower temperatures than OH.

(*f*) *CH distributed in Spiral Arms*

When the CH cloud is at a different kinematic distance from that of the continuum source, the assumption of a uniform CH cloud larger than the beam and source (case (iv) in subsection (*c*) above) might be reasonable. Rydbeck *et al.* (1975) have mapped the CH emission on and around Cas A. All three CH lines increase considerably in intensity when observed in the direction of this source, clearly demonstrating weak maser amplification. For the Orion arm cloud, Rydbeck *et al.* deduce the following transition temperatures:

$$T_{11} = -16\,\mathrm{K}, \qquad T_{01} = -8\,\mathrm{K}, \qquad T_{10} = -10\,\mathrm{K}.$$

This shows greater population inversion for the satellite lines than for the main line and is similar to the result for the dark clouds. The Cas A observations show that the opacities are very small, with $\tau \approx -0{\cdot}001$. The CH column density is found to be $\sim 10^{13}\,\mathrm{cm}^2$. Comparison with OH and H_2CO absorption data leads to

$$N_{\mathrm{CH}}:N_{\mathrm{OH}}:N_{\mathrm{H_2CO}} \approx 1:4:0{\cdot}1\,.$$

The approximate equality of T_{01} and T_{10} in dark clouds and in regions of the Galaxy well away from continuum sources contrasts with the behaviour in the vicinity of HII regions, where $|T_{01}|$ is usually found to be considerably less than $|T_{10}|$, that is, $T_{\mathrm{L}}(3264)$ is considerably greater than $T_{\mathrm{L}}(3349)$. The different behaviour is well illustrated in the Onsala results (Rydbeck *et al.* 1975) for the main component G49·5−0·2 of W51 for the two velocities of $+5\,\mathrm{km\,s^{-1}}$ (CH near the Sun) and $+64\,\mathrm{km\,s^{-1}}$ (CH near the HII region), shown in their Figs 24 and 25. The line ratio $T_{\mathrm{L}}(3264)/T_{\mathrm{L}}(3349)$ is considerably greater at $64\,\mathrm{km\,s^{-1}}$ than at $5\,\mathrm{km\,s^{-1}}$, in keeping with the present results.

5. Conclusions

The F = 0–1 transition at 3264 MHz has been looked for in 20 positions, mainly in the direction of HII regions, and detected in emission in 16 sources; the F = 1–1 transition at 3335 MHz was looked for in 16 positions and detected in 7, 5 of which were in absorption; the F = 1–0 transition at 3349 MHz was looked for in 3 positions, but not definitely detected. The median value of $T_{\mathrm{L}}/T_{\mathrm{c}}$ was 0·021 at 3264 MHz and −0·010 at 3335 MHz. Where absorption at 3335 MHz accompanied emission at 3264 MHz, the ratio $T_{\mathrm{L}}(3335):T_{\mathrm{L}}(3264)$ had a mean value of $-1:2{\cdot}5$; the corresponding ratio of transition temperatures would be $-5:1$. However, because of the severe sensitivity limitations of the survey any statistics are greatly influenced by selection effects.

When the present results are combined with those already published it appears that all three transitions are usually inverted, but that in the vicinity of bright HII regions the inversion of the F = 0−1 transition is increased while that of the F = 1−1 transition is decreased and in extreme cases absorption occurs. The transition temperature T_{11} might then be as low as 50 K. We have suggested that this reversal occurs in regions of high density.

Column densities of CH are in the vicinity of $10^{14}\,\mathrm{cm^{-2}}$, and in some instances may be as high as for OH. The values are roughly comparable with the optically derived values. The CH probably occurs in spiral arm features in the Galaxy with a distribution similar to HI in absorption. There is no correlation between apparent optical depths of CH and those of OH or H_2CO, and there is no CH enhancement in the centre of the Galaxy.

For the future, more accurate mapping of CH distributions is very desirable, both where the CH is associated with the continuum sources and where it is not (the $-22\ \mathrm{km\,s^{-1}}$ feature in G326·7+0·6 is in the latter category). Attempts should also be made to detect transitions of the higher states, the $^2\Pi_{1/2}, J = 3/2$ and the $^2\Pi_{3/2}, J = 5/2$, which are only 18 and 67 $\mathrm{cm^{-1}}$ above the ground state and so likely to be populated. Estimates of the corresponding frequencies are about 500 and 7200 MHz.

References

Burdyuzha, V. V., and Varshalovich, D. A. (1973). *Sov. Astron.* AJ **16**, 980.
Gardner, F. F., and Robinson, B. J. (1974). *Proc. Astron. Soc. Aust.* **2**, 253.
Gwinn, W. D., Turner, B. E., Goss, W. M., and Blackman, G. L. (1973). *Astrophys. J.* **179**, 789.
Hjalmarson, A., *et al.* (1975). Onsala Space Observ. Res. Rep. No. 124.
Kutner, M., and Thaddeus, P. (1971). *Astrophys. J.* **168**, L67.
Manchester, R. N., Robinson, B. J., and Goss, W. M. (1970). *Aust. J. Phys.* **23**, 751.
Robinson, B. J. (1974). Proc. IAU Symp. No. 60 on Galactic Radio Astronomy, p. 521 (Reidel: Dordrecht, Holland).
Robinson, B. J., Gardner, F. F., Sinclair, M. W., and Whiteoak, J. B. (1974). *Nature* (*London*) **248**, 31.
Rydbeck, O. E. H, Elldér, J., and Irvine, W. M. (1973). *Nature* (*London*) **246**, 466.
Rydbeck, O. E. H., Elldér, J., Irvine, W. M., Sume, A., and Hjalmarson, A. (1974). *Astron. Astrophys.* **33**, 315.
Rydbeck, O. E. H., Kollberg, E., Hjalmarson, A., Sume, A., Elldér, J., and Irvine, W. M. (1975). Onsala Space Observ. Res. Rep. No. 120.
Turner, B. E., and Zuckerman, B. (1974). *Astrophys. J.* **187**, L59.
Whiteoak, J. B., and Gardner, F. F. (1974). *Astron. Astrophys.* **37**, 389.
Zuckerman, B., and Turner, B. E. (1975). *Astrophys. J.* **197**, 123.

Manuscript received 3 November 1975